Received: 30 May 2017 | Revised: 12 April 2018 | Accepted: 24 April 2018

DOI: 10.1002/nbm.3946

RESEARCH ARTICLE

WILEY NMR IN BIOMEDICINE

Impact of contrast agent injection duration on dynamic contrast-enhanced MRI quantification in prostate cancer

Edzo M.E. Klawer[1] | Petra J. van Houdt[1] | Floris J. Pos[1] | Stijn W.T.P.J. Heijmink[2] | Matthias J.P. van Osch[3] | Uulke A. van der Heide[1]

[1] Department of Radiation Oncology, The Netherlands Cancer Institute, Amsterdam, The Netherlands

[2] Department of Radiology, The Netherlands Cancer Institute, Amsterdam, The Netherlands

[3] Department of Radiology, Leiden University Medical Centre, Leiden, The Netherlands

Correspondence
Uulke A. van der Heide, The Netherlands Cancer Institute, Department of Radiation Oncology, Plesmanlaan 121, 1066 CX Amsterdam, The Netherlands.
Email: u.vd.heide@nki.nl

Funding information
Dutch Cancer Society, Grant/Award Number: NKI2013-5937

The volume transfer constant K^{trans}, which describes the leakage of contrast agent (CA) from vasculature into tissue, is the most commonly reported quantitative parameter for dynamic contrast-enhanced (DCE-) MRI. However, the variation in reported K^{trans} values between studies from different institutes is large. One of the primary sources of uncertainty is quantification of the arterial input function (AIF). The aim of this study is to determine the influence of the CA injection duration on the AIF and tracer kinetic analysis (TKA) parameters (i.e. K^{trans}, k_{ep} and v_e).

Thirty-one patients with prostate cancer received two DCE-MRI examinations with an injection duration of 5 s in the first examination and a prolonged injection duration in the second examination, varying between 7.5 s and 30 s. The DCE examination was carried out on a 3.0 T MRI scanner using a transversal T_1-weighted 3D spoiled gradient echo sequence (300 s duration, dynamic scan time of 2.5 s). Data of 29 of the 31 were further analysed. AIFs were determined from the phase signal in the left and right femoral arteries. K^{trans}, k_{ep} and v_e were estimated with the standard Tofts model for regions of healthy peripheral zone and tumour tissue.

We observed a significantly smaller peak height and increased width in the AIF for injection durations of 15 s and longer. However, we did not find significant differences in K^{trans}, k_{ep} or v_e for the studied injection durations. The study demonstrates that the TKA parameters K^{trans}, k_{ep} and v_e, measured in the prostate, do not show a significant change as a function of injection duration.

KEYWORDS

arterial input function, contrast agent, dynamic contrast-enhanced MRI, injection protocol, K^{trans}, phase signal, prostate cancer, tracer kinetic analysis

Abbreviations: AIF, arterial input function; AUC_{300}, area under the curve over the full acquisition; CA, contrast agent; CTC, concentration–time curve; DCE-MRI, dynamic contrast-enhanced MRI; FWHM, full width at half maximum; k_{ep}, flux rate constant; K^{trans}, transfer constant; ROI, region of interest; SNR, signal to noise ratio; TKA, tracer kinetic analysis; v_e, volume of extravascular extracellular space; VFA, variable flip angle; wCV, within-subject coefficient of variation.

1 | INTRODUCTION

Dynamic contrast-enhanced (DCE-) MRI is a minimally invasive method for tumour characterization, localization and therapeutic response assessment.[1] It enables quantification of perfusion and permeability of the tissue microvasculature by tracer kinetic analysis (TKA). DCE-MRI is a valuable diagnostic addition for the detection of tumour tissue in prostate, because tumour growth is associated with neovascularization.[2,3]

The volume transfer constant K^{trans}, which describes the leakage of contrast agent (CA) into tissue,[4] is the most commonly reported quantitative parameter for DCE-MRI. However, the variation in K^{trans} values between studies from different institutes is large.[2,5] These differences in resulting TKA parameters make it harder to assess real changes over time for treatment response monitoring[6] or compare results between MR studies.[2] The variations are related to the complexity and variety of choices that are possible in both the acquisition and analysis of DCE-MRI data, such as dose, concentration and type of CA,[7] pre-contrast T_1 mapping,[8] partial volume corrections,[9] kinetic model choice,[10] fitting procedures, tumour site and, as one of the main contributors to variation, the arterial input function (AIF).[11,12] Here we focused on the injection protocol. The aim of this study is to determine the influence of the CA injection duration on the AIF and TKA parameters (i.e. K^{trans}, k_{ep} and v_e).

The AIF is influenced by factors such as the duration and dose of contrast injection, the cardiac output and the distribution of the CA throughout the body.[13] The influence of variations in injection protocol settings in combination with the dynamic interval time and duration of the acquisition has been investigated with simulation studies for DCE-MRI[14-16] and with simulation and experimental studies in animal models for DCE-CT.[17-19] These studies showed that tissue contrast enhancement curves and TKA parameters strongly depend on the injection protocol. Increased injection duration resulted in lower contrast enhancement in tissue. The most reliable TKA estimation was achieved with high injection volumes (45 mL).[14] These findings are supported by animal studies.[17,19-21] However, the influence of the injection duration on the AIF and TKA parameters has not been investigated in patient studies. Therefore, in this study we investigated the effect of variations in injection duration on the AIF and TKA parameters in prostate cancer.

2 | METHODS

2.1 | Patients

Thirty-one patients with biopsy-proven prostate cancer, assigned for external beam radiation therapy and eligible to undergo an MRI examination, were included (median age 71, range between 59 and 83 years). Patients previously treated for prostate cancer or treated with hormonal therapy were excluded. All patients received a multi-parametric MRI examination on two separate days (time interval 3–14 days). The examinations were performed between May 2013 and May 2014. The institutional review board approved this study and all patients gave written informed consent.

2.2 | Imaging protocol

All patients received a multi-parametric MRI examination on a 3.0 T MRI scanner (Achieva, Philips, The Netherlands) using a six-channel phased-array cardiac coil, according to the ESUR guidelines.[22] The examination contained three orthogonal T_2-weighted MRI scans, a T_1-weighted MRI, diffusion-weighted MRI and DCE-MRI. The transversal T_2-weighted scan was acquired with a turbo spin echo sequence (field of view 284 × 390 mm^2, acquired voxel size 0.7 × 0.7 × 3 mm^3, reconstructed voxel size 0.4 × 0.4 × 3 mm^3, repetition time (T_R) 3135–3738 ms, echo time (T_E) 120 ms).

The DCE-MRI was acquired using a transversal T_1-weighted 3D spoiled-gradient echo sequence with the following parameters: field of view 262 × 262 × 60 mm^3, acquired voxel size 2 × 2 × 6 mm^3, reconstructed voxel size 1.4 × 1.4 × 3 mm^3, T_R 4.0 ms, T_E 1.9 ms, flip angle 13 degrees, parallel imaging factor 2 and dynamic scan time 2.5 s. The total acquisition time was 5 min. In the third dynamic scan, 7.5 mmol gadoteric acid (Dotarem, Guerbet, France, 15 mL) was injected with a power injector with an overall injection duration of 5 s in the first examination, followed by a 30 mL saline flush with the same injection rate.

In the second examination, the same amount of CA was injected; however, the injection duration was extended compared with the standard injection duration. Five different injection durations were investigated: 7.5 s (n = 8), 10 s (n = 8), 15 s (n = 5), 20 s (n = 5) and 30 s (n = 5).

To convert the DCE-MRI signal intensities into concentration values, a pre-contrast variable flip angle (VFA) series was acquired (flip angles 3, 6, 10, 20 and 30 degrees) using a similar 3D spoiled-gradient echo sequence (T_R/T_E 8.0/4.0 ms).

2.3 | Image processing

We selected regions of interest (ROIs) in the tumour and in healthy tissue to obtain a range of TKA values in prostate. Delineations were carried out on the T_2-weighted image of the first examination. We delineated the tumour ROI as the entire volume indicated by the radiologists according to the PI-RADS v2 criteria,[22] which could be on multiple contiguous slices. The ROIs of healthy tissue were delineated typically on the same slices, but on the other side of the prostate and excluding haemorrhage areas. For each examination, we visually inspected whether there was intra-session movement of the prostate between the T_2-weighted scan and the DCE scan. If this was the case, we applied rigid registration to correct these shifts. For the second examination we made sure that we covered the same volume as the first examination. To this end, we carried out a local deformable registration of the T_2-weighted MRI of the second examination to the first examination with b-spline deformations using the

correlation ratio as a cost function. Next, the delineations from the first examination were transferred to the second examination. If small registration errors remained, e.g. projecting the delineations outside the prostate border, minor manual adjustments were made.

The analysis was performed using MATLAB R2015a (MathWorks, Natick, MA, USA) in combination with in-house built algorithms. Prior to the analysis, the DCE scan was smoothed with a Gaussian filter with a standard deviation of 2.8 mm (two voxels).

2.4 | Measurement of the AIF

The AIFs were extracted from the phase signal $\Delta\varphi$ using the method described by Akbudak et al.[23] The phase signal was chosen instead of the magnitude signal, since phase is less sensitive to B_1-field inhomogeneities,[24,25] inflow artefacts[25-27] and T_2*-effects at higher concentrations.[28-30] The phase signal ($\Delta\varphi$) dependence on CA concentration is described by

$$\Delta\varphi = \gamma\frac{\Delta \boldsymbol{B}\cdot\boldsymbol{H_0}}{\|\boldsymbol{H_0}\|}T_E = \omega_0\chi_M FCT_E \tag{1}$$

with γ the gyromagnetic ratio, $\Delta\boldsymbol{B}$ the change of the magnetic induction vector, $\boldsymbol{H_0}$ the static external magnetic field vector, ω_0 the resonance frequency, χ_M the molar susceptibility of the CA, C the concentration of the CA and the geometric factor F given by

$$F = \frac{1}{3}-\frac{1}{2}sin^2\theta \tag{2}$$

where θ is the angle between the delineated femoral artery and the main magnetic field. ROIs were delineated in the left and right femoral arteries using the dynamic scan with peak enhancement for maximum contrast of the arteries with the surrounding tissue. We selected ROIs in a straight part of the arteries, without bends and bifurcations in order to extract the angle θ (Equation (2)). For both left and right femoral arteries we consistently selected the ROIs either before or after the bifurcation. For each time point, all voxels within the ROIs were averaged. Possible phase drift was corrected by defining a reference region in fatty tissue close to the artery.[29] The reference signal was smoothed with a Butterworth filter, using a cut-off frequency of 0.05 Hz, and subsequently subtracted from the AIFs. An average AIF was calculated from the left and right AIFs. This was fitted with a functional form, consisting of a Gaussian and an exponential modulated with a sigmoid function.[31] For each fitted AIF the following curve characteristics were derived: the peak height, the full width at half maximum (FWHM) and the area under the curve over the full acquisition (AUC_{300}).

2.5 | Tracer kinetic model analysis

First, a T_1 map was calculated from the VFA series with a non-linear least squares fitting procedure[32,33] based on the method of Wang et al.[34] Subsequently, median signal intensities for each tumour and healthy ROI of the DCE scan were converted to concentration–time curves (CTCs), using the method of Schabel and Parker.[35] The volume transfer constant (K^{trans}), the extracellular extravascular space volume fraction ($v_e = K^{trans}/k_{ep}$) and the rate constant (k_{ep}) from the standard Tofts model[4] were then derived from these CTCs using the method of Murase.[36] This method does not take into account the differences in bolus arrival time for AIF and CTCs. Therefore, we estimated the time before enhancement with a regression model as proposed by Cheong et al.[37] A linear-linear piecewise continuous function was fitted to the first 25 points of the CTC. It consisted of a straight line with slope zero to fit the baseline part and a line with a slope greater than zero to fit the rising part of the CTC. The time point where these two lines intersect is assumed to be the bolus arrival time.

2.6 | Simulation study

In order to investigate the impact of the measured AIFs on a wider range of TKA parameters, simulated CTCs were created with the standard Tofts model using $v_e = 0.3$,[38] and five different K^{trans} values (0, 0.125, 0.25, 0.375 and 0.50 min^{-1}). This was done by calculating an average AIF for each injection duration group (5 s, 7.5 s, 10 s, 15 s, 20 s and 30 s). The CTCs were calculated using

$$C_t(t) = K^{trans}e^{-\frac{K^{trans}}{v_e}\cdot t}\otimes C_p(t-\Delta T) \tag{3}$$

with C_t representing the simulated CTC, C_p the averaged AIF for each group and ΔT the time delay of the tissue enhancement relative to the AIF, which we set to zero for the simulations. The symbol $\otimes$ denotes the convolution operation. Random Gaussian noise with a variance of 2.3×10^{-4} was added to the CTCs to achieve a realistic signal to noise ratio (SNR). This noise level was similar to the noise level in our patient data set, defined as the standard deviation in the first five frames prior to contrast arrival. The SNR level was sufficiently high that Gaussian-distributed noise could be used, instead of a Rician distribution.[39] The TKA was repeated 100 times with random noise.

2.7 | Statistical analysis

The curve characteristics of the AIF (i.e. peak height, FWHM and AUC_{300}) were compared pairwise between the injection duration groups, using a Kruskal-Wallis pairwise non-parametric comparison test. The same test was used to investigate differences in TKA parameter values between the different injection durations. A post hoc multiple comparison test was applied to determine which injection duration resulted in significantly different TKA parameter values compared with the values of 5 s injection duration. To investigate differences between tumour and healthy tissue within the

same injection duration group of 5 s, a Wilcoxon rank sum test was applied. In the simulation study we pooled all the K^{trans} values from one injection duration (100 experiments × five input K^{trans} values) and applied a Kruskal-Wallis test to determine whether the estimated K^{trans} values were different between the injection durations. For all statistical tests, a p value less than 0.05 was considered statistically significant.

3 | RESULTS

3.1 | Patients

Two patients were excluded from further analysis. One patient had a trans-urethral resection after his first MRI examination. The DCE data of the other patient contained severe motion artefacts. Both patients were in the 10 s group, reducing the number of patients in this group from eight to six. For 26 of the remaining 29 patients, both healthy tissue ROIs in the peripheral zone and tumour tissue were defined. In two patients, from the 10 s and 15 s groups, only tumour tissue was present, and in one patient, from the 7.5 s group, no tumour could be delineated due to post-biopsy haemorrhage.

3.2 | AIF

As an example, Figure 1 shows the AIFs (measured data and fit) of a patient from the 30 s group. In the supplementary data, examples of patient AIFs (measured data and fit) are shown for the other injection durations. From this figure we observe that the peaks become lower and broader for longer injection durations. The AIF characteristics are summarized in Table 1 for each injection duration. For injection durations of 7.5 and 10 s differences in AIF characteristics were not significant. This is also demonstrated by the plots in Figure 2. For injection durations of 15 s and longer, the peak height was significantly less than that for the 5 s injection duration ($p < 0.01$), decreasing from 5.8mM for 5 s to 3.5mM for 30 s. For the injection duration of 30 s, the FWHM was significantly larger in comparison with that of the 5 s duration ($p < 0.001$); the FWHM was broadened from 9.8 s for the 5 s to 29.5 s for the 30 s injection duration.

3.3 | Effect on TKA

We assessed the registration error of the two MRI examinations by identifying corresponding landmarks. In 14 patients, small registration errors remained, e.g. projecting the delineations outside the prostate border. In this group, the registration average error was 1.7 ±0.9 mm. For these patients minor adjustments to the delineations were made.

Examples of the CTCs of healthy and tumour tissue are shown in Figure 1 for a patient of the 30 s group. The median K^{trans} for tumour tissue (0.13 [0.03–1.36] min^{-1}) was significantly higher for the standard injection duration than for healthy peripheral zone tissue (0.08 [0.03–0.39] min^{-1}) ($p = 0.01$). The median k_{ep} and v_e were not significantly different between tumour tissue and healthy tissue. The median k_{ep} was 0.51 [0.11–2.5] min^{-1} for tumour tissue and 0.55 [0.07–1.29] min^{-1} for healthy tissue, whereas v_e was 0.22 [0.05–2.6] for tumour tissue and 0.18 [0.05–0.47] for healthy tissue. The differences in TKA parameters between different injection durations are summarized in Table 2 and were not significantly related to the injection duration (range of p-values 0.09–0.85). Table 2 also shows that for some groups the range in the differences is large. Figure 3 shows the individual patient results for one of the TKA parameters, K^{trans}, illustrating that the variation is not related to the injection duration.

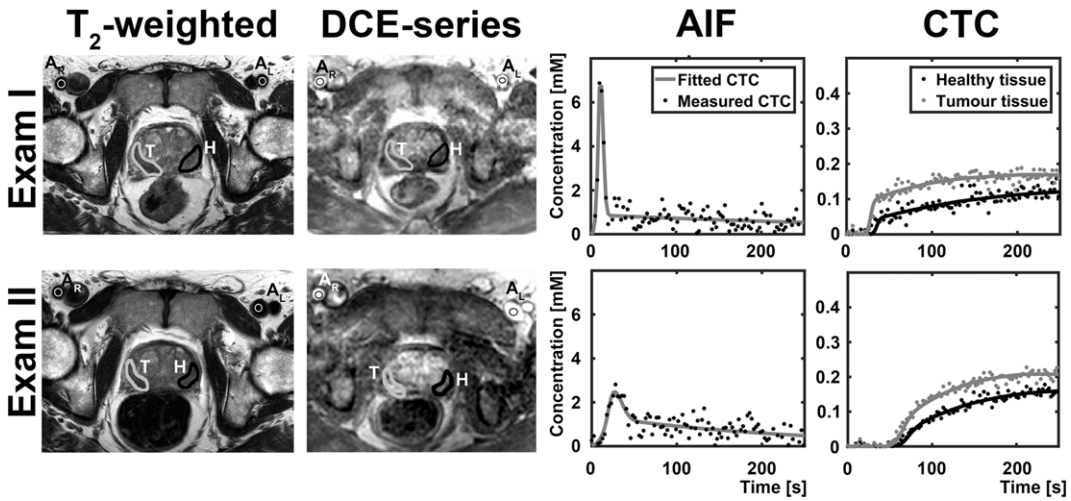

FIGURE 1 Example of a patient who was included in the 30 s injection duration group. The top row shows the T_2-weighted scan including delineations, DCE scan including delineations, AIF and CTCs for the standard injection duration, whereas the bottom row shows the scans and results for the 30 s injection duration. In the first two columns, delineations represent the left (A_L) and right (A_R) femoral arteries, tumour (T) and healthy (H) tissue. In the third column the phase signal of the AIF is plotted together with the fitted AIF. In the last column, an average CTC of tumour tissue and healthy tissue is plotted (dots) together with the fit by the standard Tofts model (solid line)

TABLE 1 The median and range for peak height, FWHM and area under the curve (AUC_{300}) are listed for the injection durations

Injection duration	Peak height [mM]		FWHM [s]		AUC_{300} [mM s]	
	median	(range)	median	(range)	median	(range)
5 s (*n* = 29)	7.3	(1.8–11.5)	9.2	(5.5–12.7)	437	(98–790)
7.5 s (*n* = 8)	7.3	(5.8–9.8)	10.9	(9.0–13.5)	401	(268–1014)
10 s (*n* = 6)	5.6	(3.2–8.5)	10.2	(9.7–119.1)	533	(358–569)
15 s (*n* = 5)	4.4	(3.1–5.7)	20.0	(16.3–24.7)	420	(275–689)
20 s (*n* = 5)	3.1	(1.5–3.8)	21.7	(20.5–30.4)	342	(164–371)
30 s (*n* = 5)	3.2	(2.3–3.8)	30.3	(29.7–128.1)	391	(240–488)

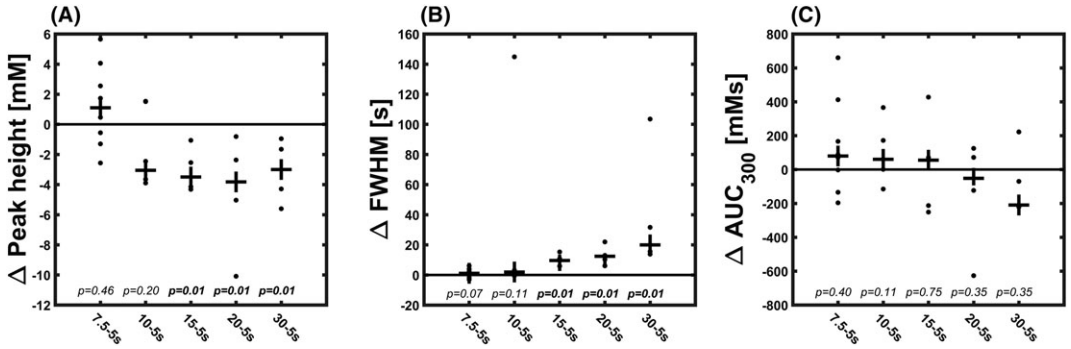

FIGURE 2 Differences in curve characteristics between the second and first examinations for each injection duration group. Individual patient results are shown by dots, whereas the median is shown by a plus sign. At the bottom of the plot the *p*-value for each group is shown. A, Change in peak height of the AIF. B, ΔFWHM of the AIF. C, Change in area under the curve (ΔAUC_{300}) of the AIF

TABLE 2 Median difference of TKA parameter estimation influenced by injection duration with respect to the 5 s duration. These differences were not significantly related to the injection duration (range of *p*-values 0.09–0.85)

Injection duration	K^{trans} [min^{-1}]		k_{ep} [min^{-1}]		v_e	
	median	(range)	median	(range)	median	(range)
Δ7.5 s–5 s	−0.03	(−0.12–0.02)	0.00	(−0.48 – −0.03)	−0.03	(−0.56–0.73)
Δ10 s–5 s	−0.03	(−0.06–0.02)	−0.24	(−1.67–0.02)	0.02	(−0.43–0.05)
Δ15 s–5 s	0.00	(−0.09–0.24)	−0.05	(−0.56 – −0.01)	−0.01	(−0.16–0.10)
Δ20 s–5 s	0.03	(−0.06–0.13)	−0.03	(−0.20 – −0.03)	−0.03	(−0.05–0.25)
Δ30 s–5 s	0.01	(−0.04–0.07)	−0.11	(−0.43–0.05)	0.05	(−0.01–0.11)

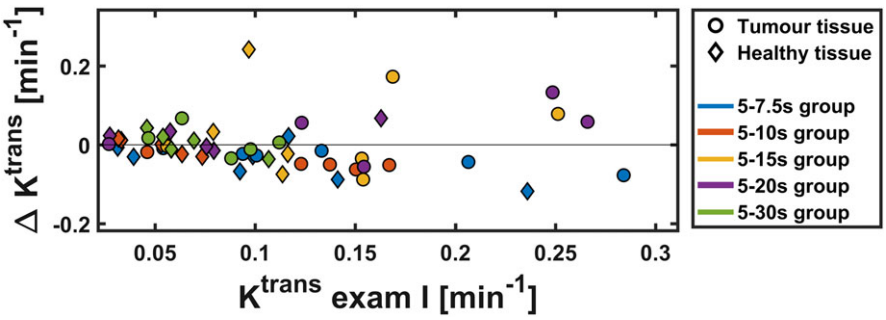

FIGURE 3 Difference in estimated K^{trans} values for different injection durations. The different injection groups are indicated by grey colour intensity. The differences between the K^{trans} values from the second and first examination (standard injection duration) are shown as a function of the K^{trans} values of the first examination

Figure 4 shows the results of the simulation study. The estimated K^{trans} values for the five longer injection durations were not significantly different from those for the 5 s injection duration ($p = 0.09$). The range of estimated K^{trans} values for the 100 experiments seems to increase for longer injection durations. Particularly for higher values of K^{trans}, we observed that the estimated K^{trans} values were significantly higher ($p < 0.001$) than the input K^{trans}. However, the relative differences were in all cases within 5%.

4 | DISCUSSION

The aim of this study was to determine the influence of the CA injection duration in DCE-MRI on the AIF and TKA parameter parameters. This is the first study to investigate the differences in human subjects. We observed significantly different AIF characteristics for injection durations of 15 s and longer. However, we did not find statistically significant differences in the values of the TKA parameters.

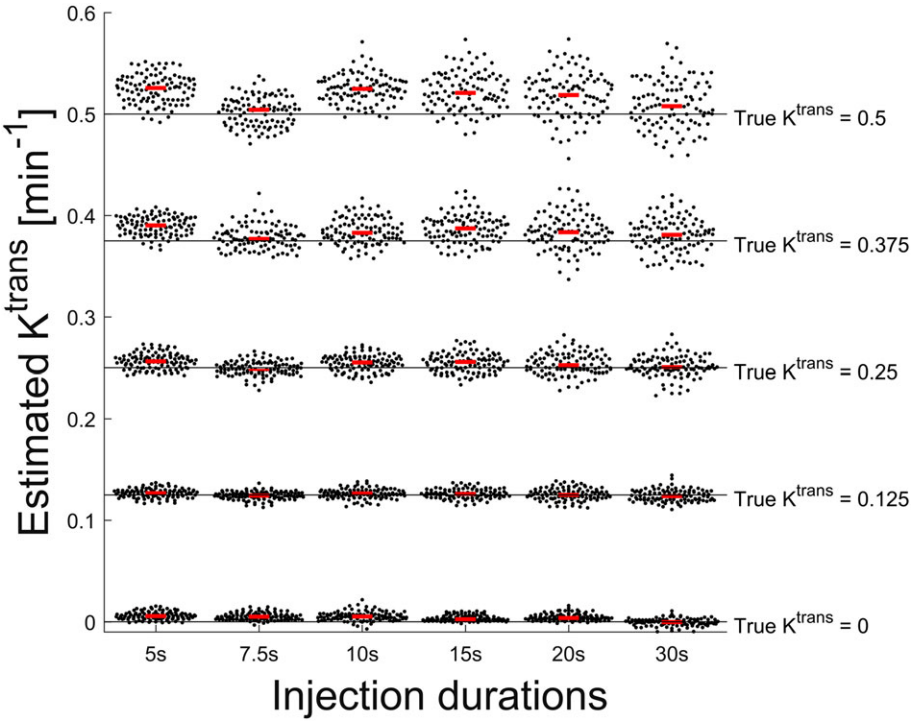

FIGURE 4 K^{trans} values derived by TKA from simulated CTCs representing the true K^{trans} values, ranging from 0 min^{-1} to 0.5 min^{-1} (right axis). Each simulated CTC (the result of TKA for a specific injection duration, representing a K^{trans} value at v_e = 0.3) was fitted 100 times (black dots). The median is shown in red

Our results show a smaller peak height and larger FWHM for AIFs when the injection duration was longer than 10 s. This is in accordance with the literature, shown in a simulation study[16] and three in vivo studies in animals.[19,21] All of these studies showed a smaller peak height, in combination with peak widening, for longer injection durations. In the simulation study by Van Osch et al., a broadening of the AIF was observed when injection durations were increased from 6 s to 15 s. A decrease to 3 s resulted in a minor sharpening of the peak width.[16]

In our patient data, the increased injection duration did not significantly affect the TKA parameter values. This is consistent with the work of Aerts et al.,[14] who showed that the value of K^{trans} did not change with varying injection rate at a fixed injection volume of 10 mL. Also under these conditions no change in the precision of the K^{trans} estimate was observed. However, the precision of the estimate of K^{trans} increased for high injection rates (5 mL/s) with a high injection volume (45 mL).[14] In the simulation study, we extended the range of K^{trans} values (0 to 0.5 min^{-1}). The effect of the injection duration on the value of K^{trans} was small. This confirms our experimental results. However, for higher K^{trans} values, the variation in estimation of K^{trans} was larger with the longer injection durations than for the 5 s group. This was not observed in our experimental results since no high K^{trans} values were found. It is however consistent with the results of Aerts et al.[14]

In this study we made two measurements per patient with standard and modified injection durations, to be able to investigate variations due to injection duration specifically and reducing the impact of variation between patients. We found that the differences in TKA parameters between two examinations with standard and longer injection durations were quite variable. This difference did not depend on the injection duration of the second examination. The variable differences may reflect the limited precision of DCE-MRI, obscuring smaller effects of injection duration. For example, Kershaw et al.[40] found a within-subject coefficient of variation (wCV) of 31% for K^{trans} in benign prostatic hyperplasia when using an AIF derived from the magnitude of the MRI signal and the adiabatic approximation to the tissue homogeneity model to fit the data. In a study by Yang et al.[41] the extended Tofts model was used and wCV values for K^{trans} between 12.5 and 15.5% were reported. Although in our study the experimental conditions changed between the two examinations, the wCV values are similar: for example, a wCV of 18% for K^{trans} in the 5–7.5 s group and a wCV of 32% for the 5–30 s group.

A limitation of our data set was that we did not have B_1 maps available to correct the flip angle for more accurate T_1 estimation. This could explain part of the intra-patient variability observed in our data set.[8] Although we applied deformable registration to match the ROIs of the two examinations, a remaining registration error could lead to small differences in ROI placement. This would also contribute to the variations in TKA values, particularly for smaller ROIs.

Another limitation in this study was the use of a fixed dose of CA. A fixed dose will result in different scalings of the AIF for patients with different weights. This does not influence a pairwise comparison of AIF parameters with different injection durations. It could however explain part of the interpatient variability as reflected in the ranges of the AIF characteristics in Table 1.

We only used the standard Tofts model, instead of examining the influence when another model was used, such as the extended Tofts model.[42,43] However, in none of the cases in our patient population did the CTCs show a sharp peak, indicating that highly vascularized tissue

was not found. In this study we only focused on TKA in prostate tissue. We cannot exclude the possibility that TKA for better perfused tissue (e.g. cancers in the head and neck region or cervix) could be more affected by injection duration differences.[42,43]

In this study we selected regions of healthy and tumour tissue to create a range of lower and higher K^{trans} values. However, relatively low K^{trans} values were found for tumour tissue, with a median of 0.13 min^{-1}, compared with reported K^{trans} values as reviewed by Gao et al.[44] They analysed 14 studies, reporting a median K^{trans} value of 0.37 min^{-1}, ranging from 0.09 to 1.26 min^{-1}). One of the explanations for these low values could be that we used an averaged CTC from the entire ROI to deal with the low concentration to noise ratio in individual voxels. This could have resulted in partial volume effects, missing parts of better perfused tissue. Furthermore, the exact location of the tumour regions could not be validated, as whole-mount section histopathological validation was not available for our patient population. We assumed no detectable difference in tumour tissue between the examinations. However, physiological differences between examinations are conceivable and could not be distinguished from the differences due to injection rates.

Another limitation of this study was that it was performed in a single centre setting. Differences in results between examinations with varying injection durations in multiple centres (different scanners and sequences) could therefore not be addressed.

In conclusion, in this study we show that injection durations of 15 s and longer result in lower and broader AIFs. However, the TKA parameters measured in prostate do not show a significant change as a function of injection duration.

ACKNOWLEDGEMENT

This project was funded by the Dutch Cancer Society (grant NKI2013-5937).

ORCID

Edzo M.E. Klawer http://orcid.org/0000-0001-9882-2149

REFERENCES

1. Shukla-Dave A, Hricak H. Role of MRI in prostate cancer detection. *NMR Biomed*. 2014;27(1):16-24.
2. Verma S, Turkbey B, Muradyan N, et al. Overview of dynamic contrast-enhanced MRI in prostate cancer diagnosis and management. *Am J Roentgenol*. 2012;198(6):1277-1288.
3. Hricak H, Choyke PL, Eberhardt SC, Leibel SA, Scardino PT. Imaging prostate cancer: a multidisciplinary perspective. *Radiology*. 2007;243(1):28-53.
4. Tofts PS, Brix G, Buckley DL, et al. Estimating kinetic parameters from dynamic contrast-enhanced T_1-weighted MRI of a diffusable tracer: standardized quantities and symbols. *J Magn Reson Imaging*. 1999;10(3):223-232.
5. van der Heide UA, Korporaal JG, Groenendaal G, Franken S, van Vulpen M. Functional MRI for tumor delineation in prostate radiation therapy. *Imag Med*. 2011;3(2):219-231.
6. Padhani AR, Miles KA. Multiparametric imaging of tumor response to therapy. *Radiology*. 2010;256(2):348-364.
7. Cuenod CA, Balvay D. Perfusion and vascular permeability: basic concepts and measurement in DCE-CT and DCE-MRI. *Diagn Interv Imaging*. 2013;94(12):1187-1204.
8. Fennessy FM, Fedorov A, Gupta SN, Schmidt EJ, Tempany CM, Mulkern RV. Practical considerations in T1 mapping of prostate for dynamic contrast enhancement pharmacokinetic analyses. *Magn Reson Imaging*. 2012;30(9):1224-1233.
9. Van Osch MJP, Van Der Grond J, Bakker CJG. Partial volume effects on aterial input functions: shape and amplitude distortions and their correction. *J Magn Reson Imaging*. 2005;22(6):704-709.
10. Duan C, Kallehauge JF, Bretthorst GL, Tanderup K, Ackerman JJH, Garbow JR. Are complex DCE-MRI models supported by clinical data? *Magn Reson Med*. 2017;77:1329-1339.
11. Garpebring A, Brynolfsson P, Yu J, et al. Uncertainty estimation in dynamic contrast-enhanced MRI. *Magn Reson Med*. 2013;69(4):992-1002.
12. Buckley DL. Uncertainty in the analysis of tracer kinetics using dynamic contrast-enhanced T_1-weighted MRI. *Magn Reson Med*. 2002;47(3):601-606.
13. Parker G, Buckley D. Tracer kinetic modelling for T1-weighted DCE-MRI. In: Jackson A, Buckley DL, Parker GJM, eds. *Dynamic Contrast-Enhanced Magnetic Resonance Imaging in Oncology*. Heidelberg, Germany: Springer; 2005:81-92
14. Aerts HJWL, van Riel NAW, Backes WH. System identification theory in pharmacokinetic modeling of dynamic contrast-enhanced MRI: influence of contrast injection. *Magn Reson Med*. 2008;59(5):1111-1119.
15. Aerts H, Jaspers K, Walter HB. The precision of pharmacokinetic parameters in dynamic contrast-enhanced magnetic resonance imaging: the effect of sampling frequency and duration. *Phys Med Biol*. 2011;56(17):5665-5678.
16. van Osch MJP, Vonken E-JPA, Wu O, Viergever MA, van der Grond J, Bakker CJG. Model of the human vasculature for studying the influence of contrast injection speed on cerebral perfusion MRI. *Magn Reson Med*. 2003;50(3):614-622.
17. Han JK, Kim AY, Lee KY, et al. Factors influencing vascular and hepatic enhancement at CT: experimental study on injection protocol using a canine model. *J Comput Assist Tomogr*. 2000;24(3):400-406.
18. Bae KT, Tran HQ, Heiken JP. Multiphasic injection method for uniform prolonged vascular enhancement at CT angiography: pharmacokinetic analysis and experimental porcine model. *Radiology*. 2000;216(3):872-880.
19. Bae KT, Heiken JP, Brink JA. Aortic and hepatic peak enhancement at CT: effect of contrast medium injection rate—pharmacokinetic analysis and experimental porcine model. *Radiology*. 1998;206(2):455-464.
20. Small WC, Nelson RC, Bernardino ME, Brummer LT. Contrast-enhanced spiral CT of the liver: effect of different amounts and injection rates of contrast material on early contrast enhancement. *Am J Roentgenol*. 1994;163(1):87-92.

21. Ahmed AS, Deuerling-Zheng Y, Strother CM, et al. Impact of intra-arterial injection parameters on arterial, capillary, and venous time–concentration curves in a canine model. *Am J Neuroradiol*. 2009;30(7):1337-1341.
22. Barentsz JO, Richenberg J, Clements R, et al. ESUR prostate MR guidelines 2012. *Eur Radiol*. 2012;22(4):746-757.
23. Akbudak E, Norberg RE, Conturo TE. Contrast-agent phase effects: an experimental system for analysis of susceptibility, concentration, and bolus input function kinetics. *Magn Reson Med*. 1997;38(6):990-1002.
24. Cheng H-LM, Wright GA. Rapid high-resolution T_1 mapping by variable flip angles: accurate and precise measurements in the presence of radiofrequency field inhomogeneity. *Magn Reson Med*. 2006;55(3):566-574.
25. Roberts C, Little R, Watson Y, Zhao S, Buckley DL, Parker GJM. The effect of blood inflow and B_1-field inhomogeneity on measurement of the arterial input function in axial 3D spoiled gradient echo dynamic contrast-enhanced MRI. *Magn Reson Med*. 2011;65(1):108-119.
26. Cheng HLM. T_1 measurement of flowing blood and arterial input function determination for quantitative 3D T_1-weighted DCE-MRI. *J Magn Reson Imaging*. 2007;25(5):1073-1078.
27. Ivancevic MK, Zimine I, Montet X, et al. Inflow effect correction in fast gradient-echo perfusion imaging. *Magn Reson Med*. 2003;50(5):885-891.
28. de Bazelaire C, Rofsky NM, Duhamel G, et al. Combined T2* and T1 measurements for improved perfusion and permeability studies in high field using dynamic contrast enhancement. *Eur Radiol*. 2006;16(9):2083-2091.
29. Garpebring A, Wirestam R, Yu J, Asklund T, Karlsson M. Phase-based arterial input functions in humans applied to dynamic contrast-enhanced MRI: potential usefulness and limitations. *Magn Reson Mater Phys Biol Med*. 2011;24(4):233-245.
30. Korporaal JG, Van Den Berg CAT, Van Osch MJP, Groenendaal G, Van Vulpen M, Van Der Heide UA. Phase-based arterial input function measurements in the femoral arteries for quantification of dynamic contrast-enhanced (DCE) MRI and comparison with DCE-CT. *Magn Reson Med*. 2011;66(5):1267-1274.
31. Parker GJM, Roberts C, Macdonald A, et al. Experimentally-derived functional form for a population-averaged high-temporal-resolution arterial input function for dynamic contrast-enhanced MRI. *Magn Reson Med*. 2006;56(5):993-1000.
32. Chang LC, Cheng GK, Basser PJ, Pierpaoli C. Linear least-squares method for unbiased estimation of T_1 from SPGR signals. *Magn Reson Med*. 2008;60(2):496-501.
33. Deoni SCL, Rutt BK, Peters TM. Rapid combined T_1 and T_2 mapping using gradient recalled acquisition in the steady state. *Magn Reson Med*. 2003;49(3):515-526.
34. Wang HZ, Riederer SJ, Lee JN. Optimizing the precision in T1 relaxation estimation using limited flip angles. *Magn Reson Med*. 1987;5(5):399-416.
35. Schabel MC, Parker DL. Uncertainty and bias in contrast concentration measurements using spoiled gradient echo pulse sequences. *Phys Med Biol*. 2008;53(9):2345-2373.
36. Murase K. Efficient method for calculating kinetic parameters using T_1-weighted dynamic contrast-enhanced magnetic resonance imaging. *Magn Reson Med*. 2004;51(4):858-862.
37. Cheong LH, Koh TS, Hou Z. An automatic approach for estimating bolus arrival time in dynamic contrast MRI using piecewise continuous regression models. *Phys Med Biol*. 2003;48:83-88.
38. Chen Y-J, Chu W-C, Pu Y-S, Chueh S-C, Shun C-T, W-YI T. Washout gradient in dynamic contrast-enhanced MRI is associated with tumor aggressiveness of prostate cancer. *J Magn Reson Imaging*. 2012;36(4):912-919.
39. Dietrich O, Raya G, Reiser MF. Magnetic resonance noise measurements and signal- quantization effects at very low noise levels. *Magn Reson Med*. 2008;60:1477-1487.
40. Kershaw LE, Hutchinson CE, Buckley DL. Benign prostatic hyperplasia: Evaluation of T_1, T_2, and microvascular characteristics with T_1-weighted dynamic contrast-enhanced MRI. *J Magn Reson Imaging*. 2009;29(3):641-648.
41. Yang C, Karczmar GS, Medved M, Oto A, Zamora M, Stadler WM. Reproducibility assessment of a multiple reference tissue method for quantitative dynamic contrast enhanced-MRI analysis. *Magn Reson Med*. 2009;61(4):851-859.
42. Ewing JR, Bagher-Ebadian H. Model selection in measures of vascular parameters using dynamic contrast-enhanced MRI: experimental and clinical applications. *NMR Biomed*. 2013;26(8):1028-1041.
43. Sourbron SP, Buckley DL. Classic models for dynamic contrast-enhanced MRI. *NMR Biomed*. 2013;26(8):1004-1027.
44. Gao P, Shi C, Zhao L, Zhou Q, Luo L. Differential diagnosis of prostate cancer and noncancerous tissue in the peripheral zone and central gland using the quantitative parameters of DCE-MRI: a meta-analysis. *Medicine*. 2016;95(52):e5715.

SUPPORTING INFORMATION

Additional supporting information may be found online in the Supporting Information section at the end of the article.

How to cite this article: Klawer EME, van Houdt PJ, Pos FJ, Heijmink SWTPJ, van Osch MJP, van der Heide UA. Impact of contrast agent injection duration on dynamic contrast-enhanced MRI quantification in prostate cancer. *NMR in Biomedicine*. 2018;31:e3946. https://doi.org/10.1002/nbm.3946